ARMY RESEARCH LABORATORY

Physics-based Modeling of a Graphene-loaded Capacitor

by Frank J. Crowne

ARL-TR-5481 **March 2011**

NOTICES

Disclaimers

The findings in this report are not to be construed as an official Department of the Army position unless so designated by other authorized documents.

Citation of manufacturer's or trade names does not constitute an official endorsement or approval of the use thereof.

Destroy this report when it is no longer needed. Do not return it to the originator.

Army Research Laboratory
Adelphi, MD 20783-1197

ARL-TR-5481 **March 2011**

Physics-based Modeling of a Graphene-loaded Capacitor

Frank J. Crowne
Sensors and Electron Devices Directorate, ARL

REPORT DOCUMENTATION PAGE

Form Approved
OMB No. 0704-0188

1. REPORT DATE *(DD-MM-YYYY)*	2. REPORT TYPE	3. DATES COVERED (From - To)
March 2011		

4. TITLE AND SUBTITLE
Physics-based Modeling of a Graphene-loaded Capacitor

5a. CONTRACT NUMBER

5b. GRANT NUMBER

5c. PROGRAM ELEMENT NUMBER

6. AUTHOR(S)
Frank J. Crowne

5d. PROJECT NUMBER

5e. TASK NUMBER

5f. WORK UNIT NUMBER

7. PERFORMING ORGANIZATION NAME(S) AND ADDRESS(ES)
U.S. Army Research Laboratory
ATTN: RDRL-SER-E
2800 Powder Mill Road
Adelphi, MD 20783-1197

8. PERFORMING ORGANIZATION REPORT NUMBER
ARL-TR-5481

9. SPONSORING/MONITORING AGENCY NAME(S) AND ADDRESS(ES)

10. SPONSOR/MONITOR'S ACRONYM(S)

11. SPONSOR/MONITOR'S REPORT NUMBER(S)

12. DISTRIBUTION/AVAILABILITY STATEMENT
Approved for public release; distribution unlimited.

13. SUPPLEMENTARY NOTES

14. ABSTRACT
In this report a mathematical model is developed for a capacitor containing a monolayer of graphene. The model can be used in a zero-order description of the terminal structure of a graphene field-effect transistor in which the gate-source and gate-drain connections are replaced by capacitances, a standard approximation used in the modeling of ordinary MOSFETs. The analysis leads to mathematical expressions for the charge density in the graphene channel. Whereas in a previous report (ARL-TR-5281) the author finessed this aspect of the transistor modeling by using an empirical model for the channel charge density, the density calculated here includes atomistic properties of the graphene layer. The treatment also allows nonlinear effects—i.e., varactor action—to be studied, which indicate that the graphene-loaded capacitor is an interesting device in its own right.

15. SUBJECT TERMS
Graphene, ambipolarity, varactor

16. SECURITY CLASSIFICATION OF:			17. LIMITATION OF ABSTRACT	18. NUMBER OF PAGES	19a. NAME OF RESPONSIBLE PERSON
a. REPORT	b. ABSTRACT	c. THIS PAGE	UU	34	Frank J. Crowne
Unclassified	Unclassified	Unclassified			19b. TELEPHONE NUMBER (*Include area code*) (301) 394-5759

Contents

List of Figures

1. Introduction

The standard approach to modeling transport-based semiconductor devices such as transistors, charge-coupled devices, etc. (*1*) begins with analysis of the device response under open-circuit conditions in the output circuit—i.e., with either an open source or an open drain contact. In the absence of lateral transport from a source to drain, these devices can be described by one-port circuits. In the case of field-effect transistors (FETs), the lack of direct current (dc) gate current makes the transistor essentially a capacitor, which greatly simplifies the full two-port device equivalent circuit. More importantly, the open-circuit response lets us find the charge density ρ in the channel as a function of gate voltage. Knowledge of ρ is sufficient to determine many other fundamental features of the transistor characteristics, for example the transistor's alternating current (ac) input impedance.

The approximate description of the aforementioned transistor can be formulated by first analyzing a purely capacitive structure in which a monolayer of graphene is embedded in the dielectric layer of a simple parallel-plate capacitor. This approach to modeling is especially fruitful in the case of graphene-based transistor structures such as the one shown in figure 1 (*2*), which shows a graphene device structure in current use. Unlike a normal field-effect transistor, this structure includes two gates, a top gate and a bottom (back) gate, both of which control the channel charge density ρ.

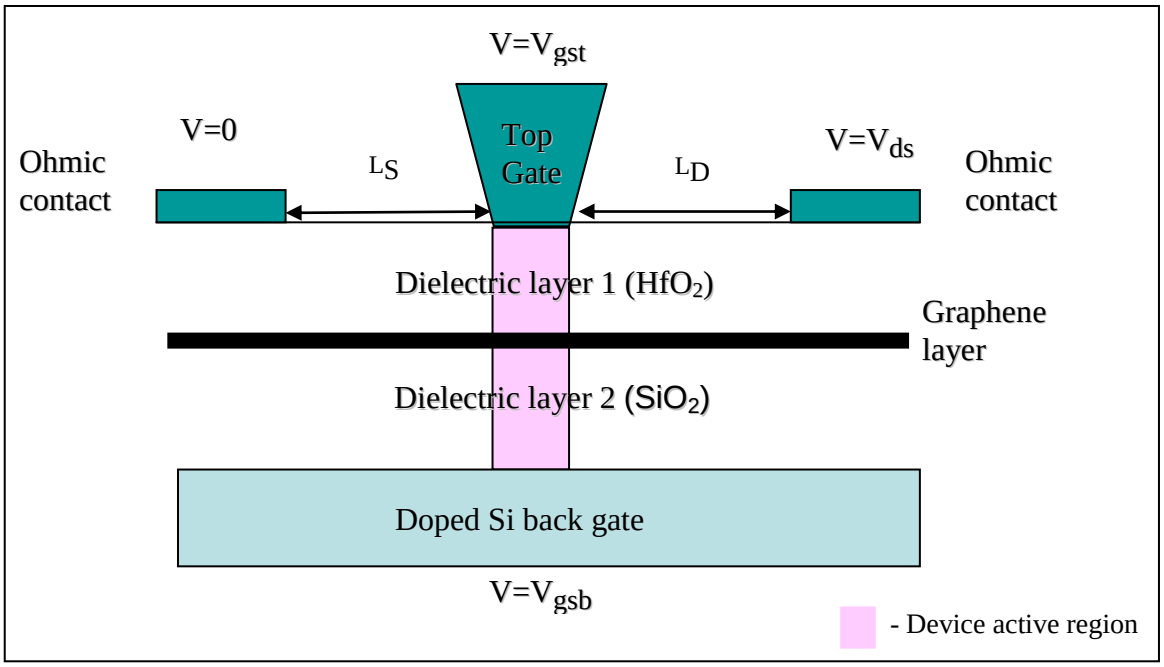

Figure 1. Dual-gate graphene FET structure.

Since graphene is ambipolar, both electrons and holes are present in the channel and contribute to the current; hence, ρ must include both species of carrier. The back gate electrode makes it possible to "dope" the FET channel *n*- or *p*-type by electrostatically generating the appropriate "inversion layers" using MOSFET terminology.

In a series of papers (*3*–*5*), Meric et al. specify the "total" charge density ρ by the following empirical expression:

$$\rho\left(V_{gst},V_{gsb}\right)=\sqrt{{\rho_0}^2+{C_{gst}}^2\left(V_{gst}-{V_{gst}}^0\right)^2+{C_{gsb}}^2\left(V_{gsb}-{V_{gsb}}^0\right)^2}\,, \qquad (1)$$

where V_{gst} and V_{gsb} are voltages applied to the top and back gates, respectively. This expression incorporates a peculiarity exhibited by graphene films: the existence of a "minimum conductivity" in the graphene channel (*6*), apparently associated with ambipolarity. Meric et al. argue in (*3*–*5*) that this minimum conductivity corresponds to a minimum charge density, ρ_0, in the channel. The expression equation 1 contains five fitting parameters: the minimum charge density ρ_0, the capacitances per unit area C_{gst} and C_{gsb} between the two gates and the monolayer, and threshold gate voltages ${V_{gsb}}^0$, ${V_{gst}}^0$ at which the minimum charge density ρ_0 is reached as the back and top gates are varied separately.

The fact that this expression has a minimum at some voltage obscures the fact that neither the number of electrons nor the number of holes has such a minimum. It, therefore, sidesteps much of the discussion of ambipolar transport. However, as we shall see, this issue must be addressed for the graphene-loaded capacitor.

2. Modeling Methodology

A rigorous expression for the channel charge density $\rho\left(V_{gst},V_{gsb}\right)$ can be obtained by modeling the multilayer structure shown in figure 2. This structure, which is related to figure 1 by a clockwise rotation of 90°, consists of a graphene monolayer located at the interface between two different dielectrics (chosen to be SiO_2 and HfO_2 by Meric et al.), with dielectric constants ε_1 and ε_2. There are two electrodes that act as gates, a back gate on the left-hand dielectric and a top gate on the right-hand dielectric. When voltages V_{gb} and V_{gt} are applied to these gates, the internal potential energy $U(x)=-qV(x)$ between them (where *q* is the charge of a single electron/hole) is a piecewise-linear function of the distance *x* through the capacitor along an axis from the back gate to the top gate. When the graphene layer is uncharged, $U(x)$ consists of two

straight line segments with a jump in slope at the interface between the dielectrics, due to the differing dielectric constants of the layers. A charge ρ on the graphene layer causes a further change in the slope. Let us write $U(x)$ as follows:

$$U(x)=\begin{cases} U_{gb}+R\left(x+\dfrac{L}{2}\right) & x\in\left[-\dfrac{L}{2},d\right] \\ U_{gt}+S\left(x-\dfrac{L}{2}\right) & x\in\left[d,\dfrac{L}{2}\right] \end{cases},$$

where the left electrode is at $x=-\dfrac{L}{2}$, the right electrode is at $x=+\dfrac{L}{2}$, and *d* is the position of the graphene monolayer. In this expression, $U_{gb}=-qV_{gb}$ is the value of the potential energy at $x=-\dfrac{L}{2}$ and $U_{gt}=-qV_{gt}$ is its value at $x=+\dfrac{L}{2}$, while *R* and *S* are constants to be determined.

At the monolayer, we have two boundary conditions:

(1) Continuity of $U(x)$ at $x=d$:

$$U_{gt}+S\left(d-\frac{L}{2}\right)=U_{gb}+R\left(d+\frac{L}{2}\right)\Rightarrow \Delta U_G=R\left(\frac{L}{2}+d\right)+S\left(\frac{L}{2}-d\right),$$

where $\Delta U_G=U_{gt}-U_{gb}$.

(2) A jump in the derivative of $U(x)$ at $x=d$, determined by the Poisson equation

$$\frac{d}{dx}\varepsilon(x)\frac{dU}{dx}=+q\rho\delta(x-d)\Rightarrow \varepsilon_2U'(d+)-\varepsilon_1U'(d-)=q\rho\Rightarrow \varepsilon_2S-\varepsilon_1R=q^2(p-n),$$

where *p* and *n* are the 2D hole and electron (number) densities in the monolayer.

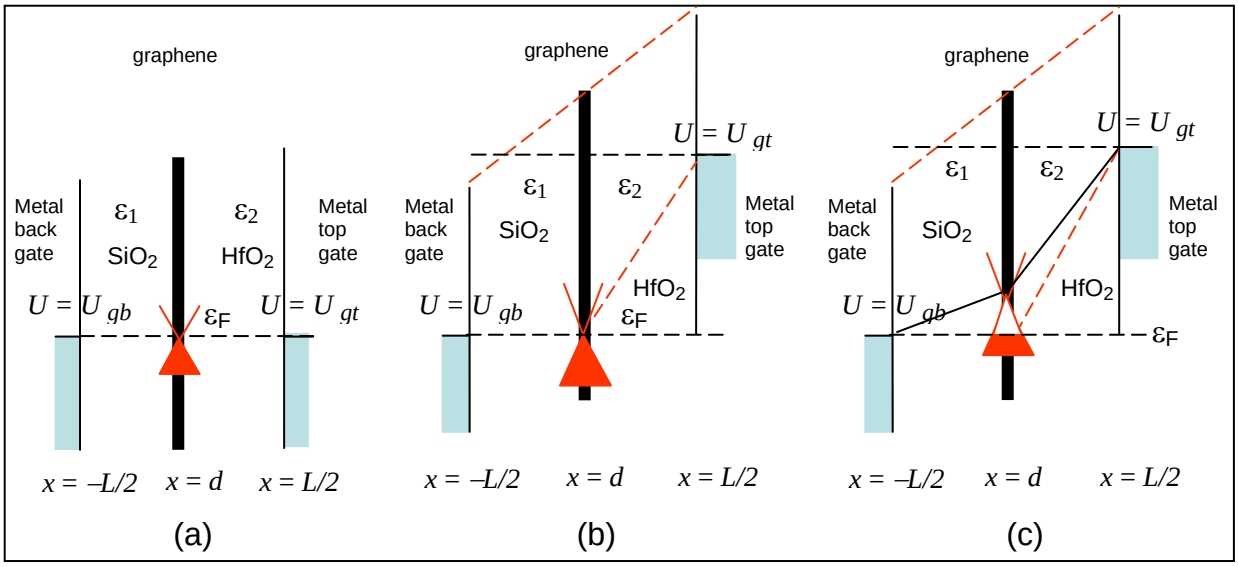

Figure 2. Graphene-loaded capacitor with a positive bias on the top gate.

Let $\Lambda = \varepsilon_1\left(\frac{L}{2}-d\right)+\varepsilon_2\left(\frac{L}{2}+d\right)$. Then solving these two equations for B and C gives

$$U(x)=\begin{cases} U_{gb}+\frac{1}{\Lambda}\left(\varepsilon_2\Delta U_g-\left[\frac{L}{2}-d\right]q^2[p-n]\right)\left(x+\frac{L}{2}\right) & x\in\left[-\frac{L}{2},d\right] \\ U_{gt}+\frac{1}{\Lambda}\left(\varepsilon_1\Delta U_g+\left[\frac{L}{2}+d\right]q^2[p-n]\right)\left(x-\frac{L}{2}\right) & x\in\left[d,\frac{L}{2}\right] \end{cases}.$$

At $x = d$ we find that

$$U(d)=\frac{1}{\Lambda}\left(\varepsilon_1\left[\frac{L}{2}-d\right]U_{gb}+\varepsilon_2\left[\frac{L}{2}+d\right]U_{gt}\right)-\left(\frac{L^2}{4}-d^2\right)\frac{q^2}{\Lambda}[p-n].$$

Let $C_{gsb}=\frac{\varepsilon_1}{\frac{L}{2}+d}$ and $C_{gst}=\frac{\varepsilon_2}{\frac{L}{2}-d}$ be the capacitances per unit area between the gates and the monolayer. Then it is easy to show that $\frac{\Lambda}{\frac{L^2}{4}-d^2}=C_{gsb}+C_{gst}$ and

$$\frac{1}{\Lambda}\left(\varepsilon_1\left[\frac{L}{2}-d\right]U_{gb}+\varepsilon_2\left[\frac{L}{2}+d\right]U_{gt}\right)=\frac{C_{gsb}U_{gb}+C_{gst}U_{gt}}{C_{gsb}+C_{gst}}$$

so that

$$U(d) = \frac{C_{gsb}U_{gb} + C_{gst}U_{gt}}{C_{gsb} + C_{gst}} - \frac{q^2}{C_{gsb} + C_{gst}}[p - n].$$

3. Carrier Statistics In Graphene

Because both electrons and holes are simultaneously present in graphene, let us pause to discuss the nature of transport in a graphene FET. Although the large-scale graphene band structure is complex, in discussing transport we may confine our attention to the conduction and valence bands of the material. In addition to being two-dimensional (2-D), the bands are *conical* in shape—i.e., the energy of an electron in the conduction band is

$$E_C(k_x, k_y) = \hbar\upsilon_F\sqrt{k_x^2 + k_y^2},$$

while the energy of an electron in the valence band is

$$E_V(k_x, k_y) = -\hbar\upsilon_F\sqrt{k_x^2 + k_y^2}.$$

Note that these bands "touch" at a single point in *k*-space $(k_x, k_y) = (0, 0)$; in the literature, this is referred to as the Dirac point. Contrast this to the case of an ordinary three-dimensional (3-D) direct-gap semiconductor, for which the energy of an electron in the conduction band is

$$E_C(k_x, k_y, k_z) = \frac{\hbar^2}{2m_C}\left(k_x^2 + k_y^2 + k_z^2\right) + \frac{1}{2}E_G,$$

while the energy of an electron in the valence band is

$$E_V(k_x, k_y, k_z) = -\frac{\hbar^2}{2m_V}\left(k_x^2 + k_y^2 + k_z^2\right) - \frac{1}{2}E_G,$$

where m_C, m_V are the conduction-band and valence-band effective masses.

3.1 Zero Temperature

The *energy* distribution functions for electrons and holes at zero temperature are simply

$$f_e(\varepsilon_e) = \Theta(\varepsilon_e - \varepsilon_F)$$
$$f_h(\varepsilon_h) = \Theta(\varepsilon_F - \varepsilon_h),$$

regardless of the dimensionality of the system. The 2-D nature of the graphene band structure enters the problem when we consider the Fermi distribution in *k*-space. For a 3-D system, the zero-temperature electron/hole distribution is a filled *sphere* of radius k_F, with k_F the Fermi wave vector. Because the electron/hole density (*n* or *p*) is the integral over this distribution, we find for 3-D bands that

$$\left.\begin{matrix} n \\ p \end{matrix}\right\} = \frac{2}{(2\pi)^3} \int_0^{k_F} 4\pi k^2 dk = \frac{{k_F}^3}{3\pi^2}$$

For a 3-D electron gas, the Fermi energy measured from the bottom of the conduction band is given by $\varepsilon_F = \frac{\hbar^2 {k_F}^2}{2m}$, implying that $\varepsilon_F \propto n^{2/3}$ or $p^{2/3}$. In contrast, the distribution at zero temperature for a 2-D system is a filled *disk* of radius k_F. Because the electron/hole density (*n* or *p*) is the integral over this distribution, we find that for a 2-D system

$$\left.\begin{matrix} n \\ p \end{matrix}\right\} = \frac{4}{(2\pi)^2} \int_0^{k_F} 2\pi k dk = \frac{{k_F}^2}{\pi}$$

For a typical III-V 2D electron gas, e.g., the channel of a GaAs/AlGaAs HEMT, the Fermi energy is again given by $\varepsilon_F = \frac{\hbar^2 {k_F}^2}{2m}$, implying that $\varepsilon_F \propto n$ or p. In contrast to these "normal" systems, the conical nature of the band structure for a graphene layer gives $\varepsilon_F = \hbar \upsilon_F k_F$, so that $\varepsilon_F = \hbar \upsilon_F (\pi n)^{1/2}$ or $\hbar \upsilon_F (\pi p)^{1/2}$.

3.2 Nonzero Temperature

Both carrier species are present at finite temperatures, due to the vanishing band gap. Let us introduce the inverse thermal energy, $\beta = \frac{1}{k_B T}$, and the usual temperature-dependent carrier energy distributions: for electrons we have (*7*)

$$n = \frac{4}{(2\pi)^2} \int_{-\infty}^{\infty} f_e(k) d^2 k = \frac{4}{2\pi^2} \int_{-\infty}^{\infty} \frac{2\pi k dk}{1 + e^{\beta(\varepsilon_e - \varepsilon_F)}}$$

$$\varepsilon_e = \hbar \upsilon_F k \Rightarrow n = \frac{2}{\pi} \int_0^{\infty} \frac{k dk}{1 + e^{\beta(\hbar \upsilon_F k - \varepsilon_F)}} = \frac{2}{\pi(\beta \hbar \upsilon_F)^2} \int_0^{\infty} \frac{u du}{1 + e^{u - \beta \varepsilon_F}} = \frac{2}{\pi(\beta \hbar \upsilon_F)^2} F_1(\beta \varepsilon_F),$$

where $F_1(x)$ is the order-1 Fermi integral. Note the factor 4, which takes into account both the spin degeneracy of the electrons and the presence of two "cones" at different points in *k*-space with identical parameters—a case of the so-called "valley degeneracy" and yet another peculiarity of graphene. Likewise, for holes we have (*5*)

$$p = \frac{4}{(2\pi)^2}\int_{-\infty}^{\infty} f_h(k)\,d^2k$$

$$\varepsilon_h = -\hbar\upsilon_F k\ ,\ f_h(k) = 1 - f_e(k) = 1 - \frac{1}{1+e^{\beta\left(-\hbar\upsilon_F k - \varepsilon_F\right)}} = \frac{1}{1+e^{\beta\left(\varepsilon_F + \hbar\upsilon_F k\right)}}$$

$$\Rightarrow p = \frac{1}{\pi^2}\int_{-\infty}^{\infty} \frac{2\pi k dk}{1+e^{\beta\left(\hbar\upsilon_F k + \varepsilon_F\right)}} = \frac{2}{\pi}\int_0^{\infty} \frac{k dk}{1+e^{\beta\left(\hbar\upsilon_F k + \varepsilon_F\right)}}$$

$$= \frac{2}{\pi\left(\beta\hbar\upsilon_F\right)^2}\int_0^{\infty} \frac{u du}{1+e^{u+\beta\varepsilon_F}} = \frac{2}{\pi\left(\beta\hbar\upsilon_F\right)^2} F_1\left(-\beta\varepsilon_F\right)$$

As noted in (*8*), the temperature dependence of "intrinsic" carriers in graphene takes a peculiar form: since the equilibrium densities of electrons and holes are the same, the Fermi level must be at zero for all temperatures. Then

$$n = p \Rightarrow np = n^2 = \frac{2}{\pi\left(\beta\hbar\upsilon_F\right)^2} F_1\left(\beta\varepsilon_F\right) \frac{2}{\pi\left(\beta\hbar\upsilon_F\right)^2} F_1\left(-\beta\varepsilon_F\right)$$

$$\rightarrow \left[\frac{2}{\pi\left(\beta\hbar\upsilon_F\right)^2} F_1(0)\right]^2 \Rightarrow n = p = \frac{2}{\pi\left(\beta\hbar\upsilon_F\right)^2} F_1(0)$$

Since $F_1(0) = \frac{\pi^2}{12}$, we find that $n = p = \frac{\pi}{6}\left(\frac{kT}{\hbar\upsilon_F}\right)^2$, i.e., the densities decrease slowly with decreasing temperature according to a square law, in contrast to the decrease predicted by the expression $n = p = n_i \exp\left(-\frac{E_G}{2kT}\right)$ in an ordinary semiconductor with bandgap E_G and intrinsic carrier concentration $n_i = 2\left(\frac{2\sqrt{m_C m_V}\,kT}{\pi\hbar^2}\right)^{3/2}$, which is exponentially rapid.

4. Charge Dynamics

Assume that the back gate is shorted to the monolayer so that charge can flow between them. Figure 2(a) shows the case of no applied voltage, for which both the Fermi level, ε_F, and the Dirac point are at the same voltage as the electrodes. Note that this situation is rather artificial since the Dirac point should lie within the energy gaps of both the insulator cladding layers—i.e., below the conduction bands (which may themselves be offset) by some "confinement energy" determined by differences in work functions. This implies that its position will be offset relative to the applied voltages, as well. Because this should only cause an uninteresting dc shift in the device response, we will ignore it here.

Let us now apply a negative voltage (positive U_{gt}) to the top gate, thereby creating a nonzero potential $U(x)$ (figure 2(b)). If the monolayer and the back gate are not connected, the field is nonzero everywhere, and the Dirac point is always at a potential $U(d) > 0$. However, if the back gate and the monolayer are connected, the applied voltage will cause charge to flow, creating a counterfield that increases until the Fermi level is constant and equal to U_{gb} everywhere to the left, resulting in the potential curve shown in figure 2(b). As a result of screening by the charge in the monolayer, the field in the region to the left is now zero. However, the following argument shows that the left-hand field is actually nonzero—i.e., the screening will be incomplete. This is true for the following reason: as the charge on the monolayer increases, the counter-field drives the potential at the monolayer (and, hence, the Dirac point) downward. But the charge added or subtracted to the monolayer also drives the Fermi level away from the Dirac point, as shown in figure 2(c). Eventually ε_F reaches zero when enough electrons are drained out of the monolayer, leaving it with a positive hole charge. However, the Fermi level and the potential are no longer the same, due to the kinetic energy μ inherent in the filled Fermi sea. Since the charge that caused the original change in the discontinuity in the voltage derivative is the same charge that produces the Fermi level displacement, it can be calculated by virtue of the relation between the Fermi level and the monolayer charge density:

$$\varepsilon_F = \mu + U(d) = 0$$

The same argument holds for holes. Figure 3(a) shows the case of no applied voltage, for which both the Fermi level ε_F and the Dirac point are again at the same voltage as the electrodes. Applying a positive voltage (negative U_{gt}) to the top gate creates a nonzero potential $U(x)$ (figure 3(b)). If the monolayer and the back gate are not connected, the field is nonzero everywhere and the Dirac point is always at a potential $U(d) < 0$. Connecting the back gate and the monolayer causes charge to flow, creating a counterfield that drives the Fermi level upward

until it equals U_{gb} everywhere to the left, resulting in the potential curve shown in figure 3(b). Again, as the charge on the monolayer increases, the counter-field drives the potential at the monolayer (and, hence, the Dirac point) upward and drives the Fermi level away from the Dirac point, as shown in figure 3(c). ε_F becomes zero when enough electrons are added to the monolayer, leaving it with a negative electron charge. Again, the Fermi level and the potential are no longer the same, due to the kinetic energy inherent in the filled Fermi sea. The added charge can be calculated by virtue of the relation between the electron Fermi level and the monolayer charge density.

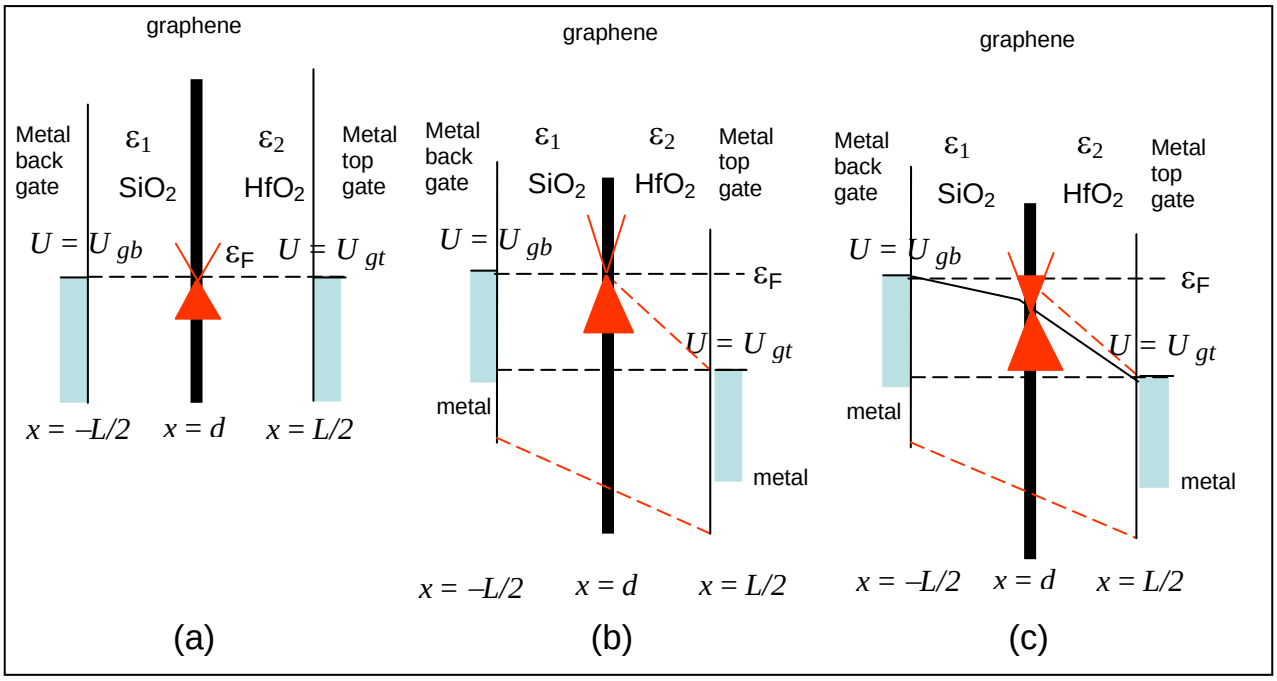

Figure 3. Graphene-loaded capacitor with a negative bias on the top gate.

4.1 Zero Temperature

When $\Delta U_g = U_{gt} - U_{gb} > 0$, figure 2 clearly shows that $\mu < U(d)$—i.e., the monolayer is charged with holes. At $T = 0$ there are no thermal electrons in the monolayer, and so $\mu = \hbar \upsilon_F (\pi p)^{1/2}$, which gives

$$\mu + U(d) = \hbar \upsilon_F (\pi p)^{1/2} + \frac{C_{gb} U_{gb} + C_{gt} U_{gt}}{C_{gb} + C_{gt}} - \frac{q^2}{C_{gb} + C_{gt}} p = 0 .$$

From the last result we can solve for *p* to obtain

$$p = \frac{1}{\pi}\left[\sqrt{A^2 + B} - A\right]^2,$$

where

$$A = \frac{\pi\hbar\upsilon_F}{2q^2}\left(C_{gb} + C_{gt}\right) \qquad B = \frac{\pi}{q^2}\left(C_{gb}U_{gb} + C_{gt}U_{gt}\right).$$

In contrast, when $\Delta U_g = U_{gt} - U_{gb} < 0$ we clearly have $\mu > U(d)$—i.e., the monolayer is charged with electrons. At $T = 0$ there are now no holes in the monolayer, and so $\mu = -\hbar\upsilon_F\left(\pi n\right)^{1/2}$, and

$$\mu + U(d) = -\hbar\upsilon_F\left(\pi n\right)^{1/2} + \frac{C_{gb}U_{gb} + C_{gt}U_{gt}}{C_{gb} + C_{gt}} + \frac{q^2}{C_{gb} + C_{gt}}n = 0,$$

from which we can solve for *n* to obtain

$$n = \frac{1}{\pi}\left[A - \sqrt{A^2 - B}\right]^2.$$

4.2 Nonzero Temperature

At finite temperatures, both carrier species are present due to the vanishing band gap. Let us introduce the inverse thermal energy, $\beta = \frac{1}{k_B T}$, and the temperature-dependent carrier distributions previously introduced. With both charges present, we write the charge density

$$\sigma = q\left(p - n\right) = \frac{2q}{\pi\left(\beta\hbar\upsilon_F\right)^2}\left\{F_1\left(-\beta\mu\right) - F_1\left(+\beta\mu\right)\right\}.$$

Note that at low temperatures, we have

$$\beta \to \infty \Rightarrow \begin{cases} \mu > 0 \Rightarrow \sigma \to \dfrac{2}{\pi\left(\beta\hbar\upsilon_F\right)^2}\left[e^{-\beta\mu} - \dfrac{1}{2}\left(\beta\mu\right)^2\right] = -\dfrac{1}{\pi}\left(\dfrac{\mu}{\hbar\upsilon_F}\right)^2 \approx -n \\ \mu < 0 \Rightarrow \sigma \to \dfrac{2}{\pi\left(\beta\hbar\upsilon_F\right)^2}\left[\dfrac{1}{2}\left(\beta\mu\right)^2 - e^{\beta\mu}\right] = +\dfrac{1}{\pi}\left(\dfrac{\mu}{\hbar\upsilon_F}\right)^2 \approx +p \end{cases},$$

which recovers the zero-temperature result. Once more we can write

$$-\mu + \frac{q^2}{C_{gt}+C_{gb}} \frac{2}{\pi\left(\beta\hbar\upsilon_F\right)^2}\left[F_1(-\beta\mu) - F_1(\beta\mu)\right] = \langle U\rangle,$$

where $\langle U\rangle = \dfrac{C_{gt}U_{gt}+C_{gb}U_{gb}}{C_{gt}+C_{gb}}$ is an "average" potential with respect to the dielectric capacitances. Once this expression is solved numerically for the Fermi energy, this energy can be used to find *n* and *p* separately:

$$p = \frac{2}{\pi\left(\beta\hbar\upsilon_F\right)^2} F_1(-\beta\mu) = p\left(\langle U\rangle\right)$$
$$n = \frac{2}{\pi\left(\beta\hbar\upsilon_F\right)^2} F_1(+\beta\mu) = n\left(\langle U\rangle\right) .$$

Figure 4 is a plot of the Fermi level versus back-gate voltage for the following parameters (*2–4*):

dielectric layers:

SiO_2 layer width:	61 nm
SiO_2 dielectric constant (ε_1):	3.9
HfO_2 layer width:	253 nm
HfO_2 dielectric constant (ε_1):	16

graphene layer

temperature:	300 K
Fermi velocity:	$1.\times 10^8$ cm/s

In figure 5, the corresponding electron and hole densities are plotted versus the back gate voltage. Note the changeover from electron to hole conduction at a back gate voltage of about –5 V.

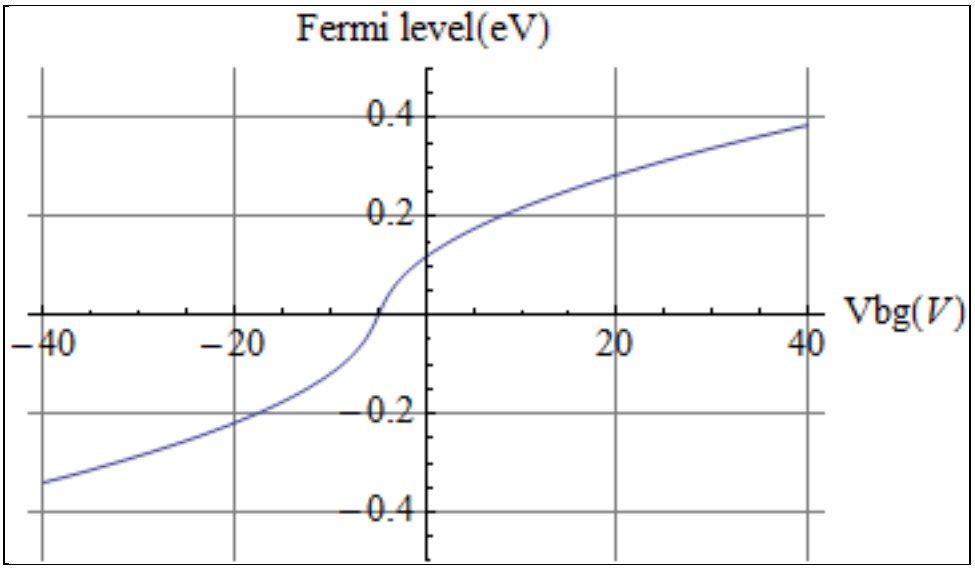

Figure 4. Fermi level versus back gate voltage Vbg.

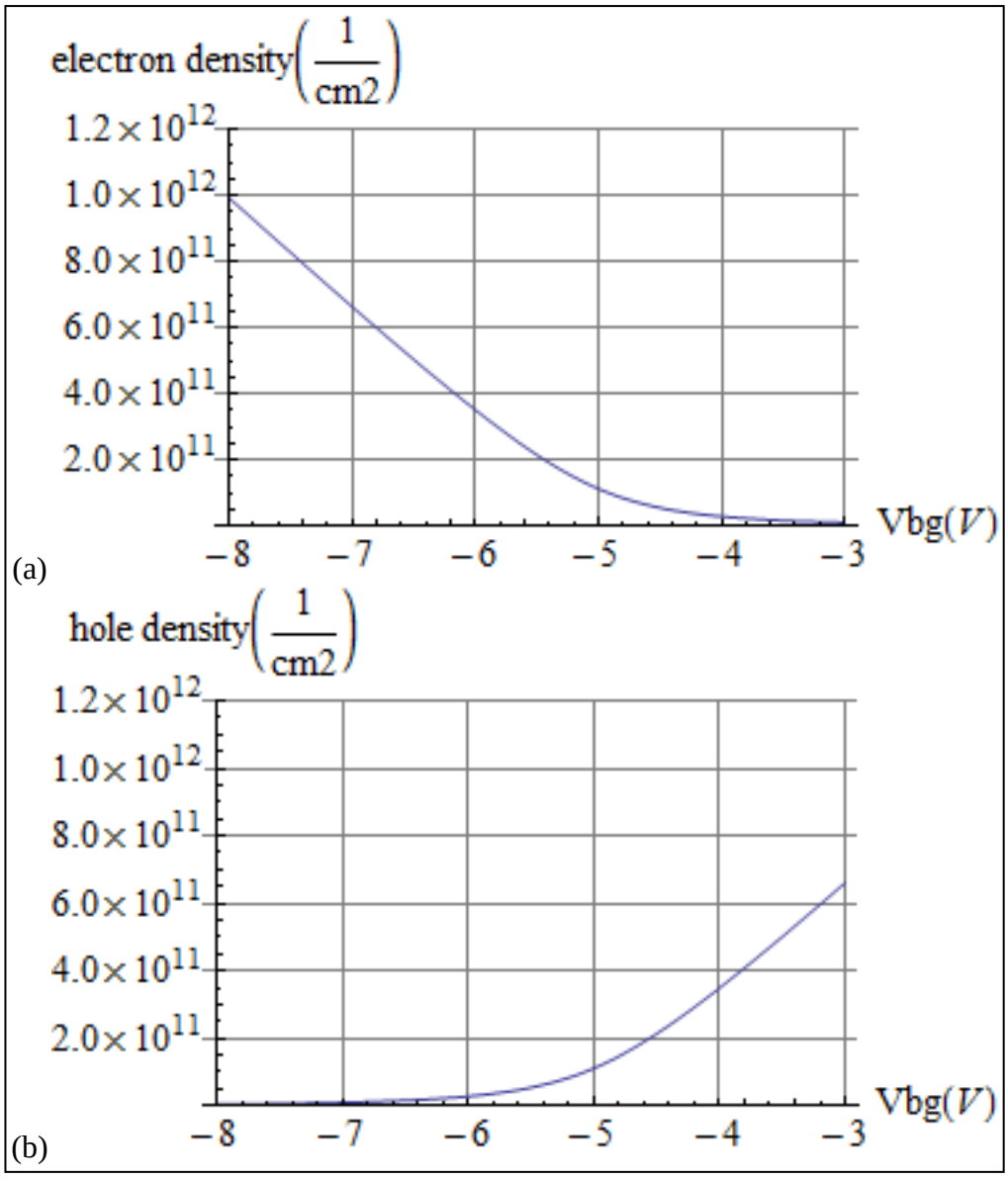

Figure 5. Electron and hole densities versus back gate voltage Vbg.

5. Nonlinear Response and Varactor Action

To find the capacitance of a graphene-loaded capacitor at finite temperatures, we need its charge-voltage relation. This follows from the relation between the Fermi level and the voltage:

$$-\mu+\frac{q^2}{C_{gt}+C_{gb}}\frac{2}{\pi\left(\beta\hbar\upsilon_F\right)^2}\left[F_1(-\beta\mu)-F_1(\beta\mu)\right]=\langle U\rangle.$$

Writing this in dimensionless form gives

$$-\beta\mu + \Lambda\left[F_1(-\beta\mu) - F_1(\beta\mu)\right] = \beta\langle U\rangle$$
$$z = \beta\mu\ ,\ \zeta = \beta\langle U\rangle \Rightarrow -z + \Lambda\left[F_1(-z) - F_1(z)\right] \equiv f(z) = \zeta\ ,$$
$$\Rightarrow z = f^{-1}(\zeta)$$

where $\Lambda = \beta\dfrac{q^2}{C_{gt}+C_{gb}}\dfrac{2}{\pi\left(\beta\hbar\upsilon_F\right)^2}$. Assume that a dc voltage is applied to the back gate of the varactor and a single-frequency ac component is applied to its top gate, i.e.,

$$\left.\begin{array}{c} U_{gb} = U_0 \\ U_{gt} = U_1\cos(\omega t + \varphi)\end{array}\right\} \Rightarrow \langle U\rangle = \frac{C_{gb}}{C_{gt}+C_{gb}}U_0 + \frac{C_{gt}}{C_{gt}+C_{gb}}U_1\cos(\omega t+\varphi)\,.$$

Let

$$\zeta_0 = \frac{C_{gb}}{C_{gt}+C_{gb}}\beta U_0 \qquad \mathrm{Z} = \frac{C_{gt}}{C_{gt}+C_{gb}}\beta\, U_1\cos(\omega t+\varphi) \equiv \zeta_1\cos(\omega t+\varphi),$$

where $\zeta_1 << \zeta_0$. Since the net charge per unit area is

$$\sigma = q(p-n) = \frac{2q}{\pi\left(\beta\hbar\upsilon_F\right)^2}\left[F_1(-\beta\mu) - F_1(\beta\mu)\right] = \left(C_{gt}+C_{gb}\right)\frac{1}{q}\left(\langle U\rangle + \mu\right) = \left(C_{gt}+C_{gb}\right)\frac{1}{\beta q}(\zeta + z)\,,$$

we can find the response once we know the function $z(\zeta)$.

The inversion of the implicit function relation $-z + \Lambda\left[F_1(-z) - F_1(z)\right] = \zeta$ can be done by power series. First, we write $z = a_0 + A(Z)$, i.e., the dc and ac parts of *z* are formally separated. Then, assuming that the function $A(Z)$ is small compared to the dc component a_0, we have the following Taylor series expansion:

$$\zeta = \zeta_0 + Z = f(z)$$
$$z = a_0 + A(Z) \Rightarrow f(z) = f(a_0) + A(Z)\,f'(a_0) + \frac{1}{2}A(Z)^2\,f''(a_0) + \frac{1}{6}A(Z)^3\,f'''(a_0)$$
$$+\frac{1}{24}A(Z)^4\,f^{iv}(a_0) + \frac{1}{120}A(Z)^5\,f^{v}(a_0) + \frac{1}{720}A(Z)^6\,f^{vi}(a_0) + \cdots$$

The derivatives of $f(z)$ are given in the appendix, which also contains mathematical details of the calculation. Expanding the function $A(Z)$ as a power series in *Z* with unknown coefficients

and matching coefficients on both sides of the expression $\zeta_0 + Z = f(z)$ leads to an expression for the function $z(\zeta)$ in powers of ζ, which can then be rewritten as a Fourier series for the charge density of the form

$$z = \sum_{m=0}^{6} c_m \cos m(\omega t + \varphi).$$

This in turn can be inserted into the charge density expression to give the varactor response:

$$\sigma = \left(C_{gt} + C_{gb}\right)\frac{1}{\beta q}\left(\zeta_0 + c_0 + \left[\zeta_1 + c_1\right]\cos(\omega t + \varphi) + \sum_{m=2}^{6} c_m \cos m(\omega t + \varphi)\right)$$

The lowest-frequency nonlinear effect is a shift in the operating point—i.e., the self-biasing effect. The "true" ac nonlinearities start with second-harmonic generation, as measured by the coefficient c_2.

Figures 6a–6e illustrate the variation of the induced surface charge density versus ac voltage at the second through sixth harmonic frequencies for an operating-point voltage $V_0 = 2$ V. It is worth noting that the charges at the even harmonics are considerable larger than those at the odd harmonics, despite the antisymmetrical shape of the overall charge-voltage curve. The explanation for this is the peculiar shape of that curve at large voltages, which is asymptotically quadratic for both signs of the voltage, but with a negative coefficient in the negative direction and a positive coefficient in the positive direction to ensure the antisymmetry. As to the numbers, since current density is the time derivative of the charge density and the harmonic densities are measured in nanocoulombs per square centimeter, we can cautiously infer that a 1 cm^2 capacitor driven at a frequency of 10 MHz could generate milliamps of ac current.

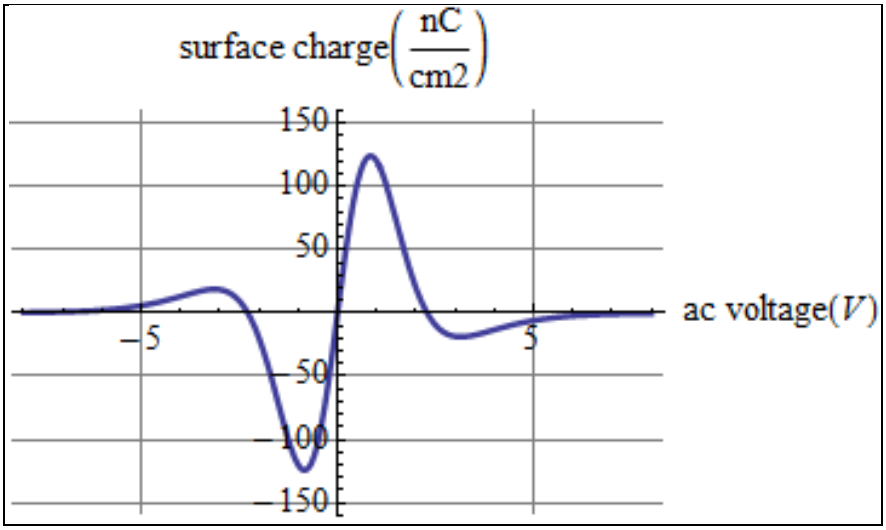

Figure 6a. 2nd harmonic surface charge density vs. ac voltage.

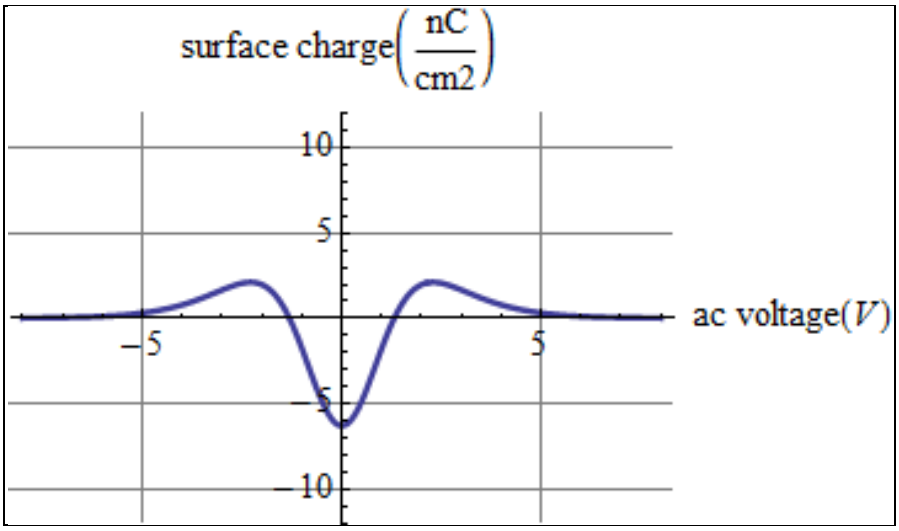

Figure 6b. 3nd harmonic surface charge density vs. ac voltage.

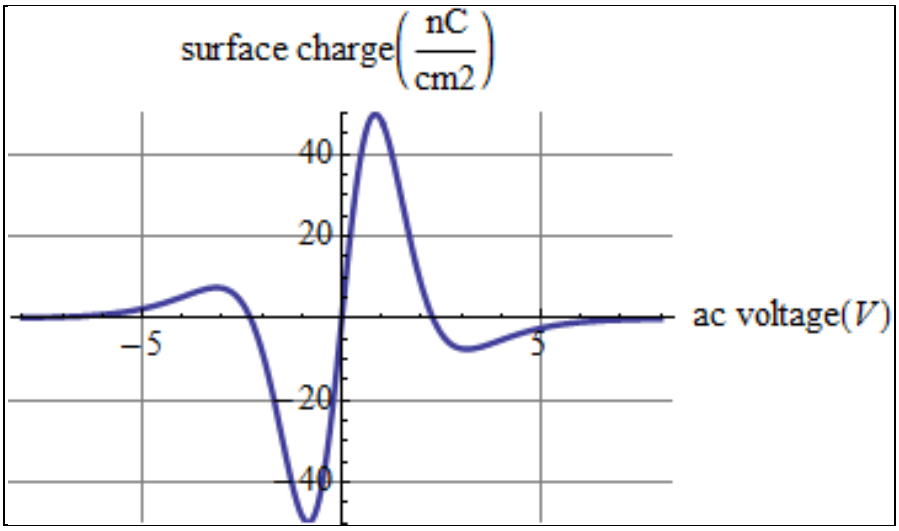

Figure 6c. 4th harmonic surface charge density vs. ac voltage.

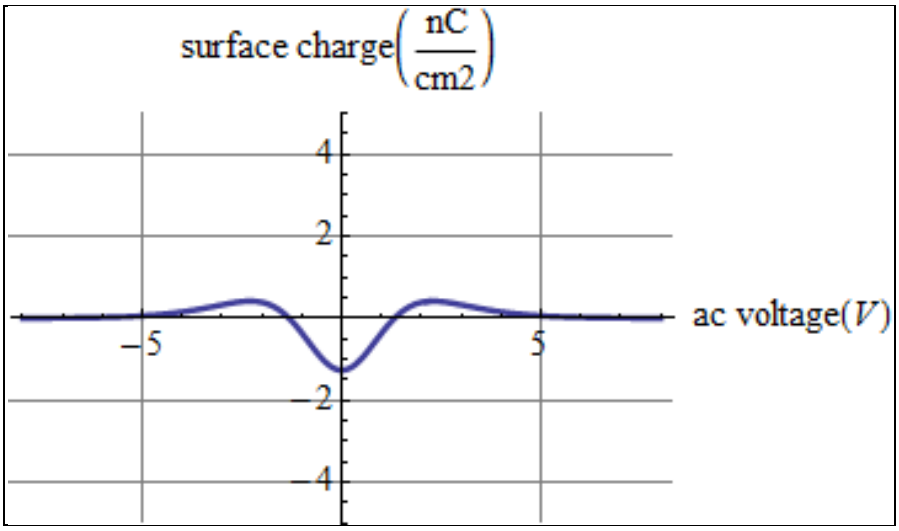

Figure 6d. 5th harmonic surface charge density vs. ac voltage.

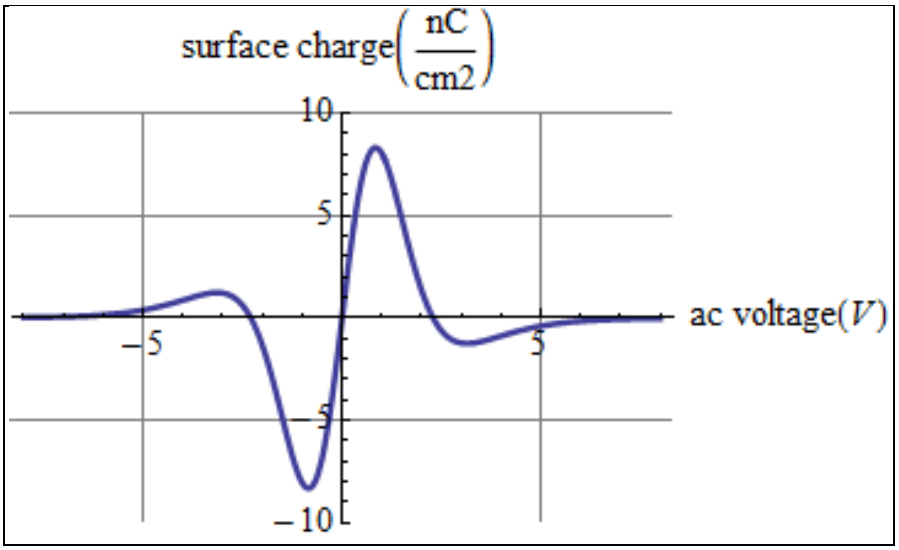

Figure 6e. 6th harmonic surface charge density vs. ac voltage.

6. Conclusions

The graphene system possesses four unusual physical features:

- two-dimensionality
- ambipolarity
- zero band gap
- a conical 2-D band structure

all of which impact the response of any device based on graphene. For this reason, analogies with other devices without all of these features can be extremely misleading. Thus, treating the graphene as if it were 3-D alters the quantum statistics, while the conical shape of the band structure (which can occur in 3-D systems, e.g., InSb) has specific implications for the energy density of states and, therefore, the charge-voltage relation. The unusual feature of ambipolarity complicates the discussion even more.

The analysis given here is of limited value as a guide to the time-dependent behavior of the device because of its quasi-dc nature: since changes in charge density cannot be instantaneous, but rather are limited by the RC time constant of the graphene material, the real device response must include discussion of the mobility of carriers in the channel, which is known to be determined by substrate material (i.e., the cladding dielectrics in this capacitor structure), as well as defect and phonon scattering in the graphene layer itself.

A further limitation on the varactor analysis is the power-series treatment of the charge-voltage relation. Fermi integrals have always been notoriously hard to deal with mathematically: pre-computer calculations tended to founder on the inability to match power series and asymptotic series for these integrals due to the "elbow bend" that is so apparent in their plots. This means that the nonlinear response of a device whose physics requires their use will only be well-described by global computations. Such computations will be the subject of future research.

7. References

1. Sze, S. M. *Physics of Semiconductor Devices;* Wiley-Interscience, New York: Wiley, 1981, 2nd ed.

2. Crowne, F. *Classical Gradual-Channel Modeling of Graphene Field-Effect Transistors (FETs)*; ARL-TR-5281; U.S. Army Research Laboratory: Adelphi, MD 20783, August 2010.

3. Meric, I.; Han, M.; Young, A. F.; Ozyilmaz, B.; Kim, P.; Shepard, K. L. *Nature Nanotechnology (Letters)* **2008**, *3*, 654.

4. Meric, I.; Han, M.; Young, A. F.; Ozyilmaz, B.; Kim, P.; Shepard, K. L. *Nature Nanotechnology (Letters)* **2008**, *3*, 654.

5. Meric, I.; Baklitskaya, N.; Kim, P.; Shepard, K. L. RF Performance of Top-gated, Zero-bandgap Graphene Field-effect Transistors. *2008 IEEE International Electron Devices Meeting* (IEEE, Piscataway, 2008), paper no. 4796738, pp. 1–4.

6. Adam, S.; Hwang, E. H.; Galitski, V. M.; Das Sarma, S. *PNAS* **November 2007**, *104* (47), 18392.

7. Fang, T.; Konar, A.; Xing, H. L.; Jena, D. *Appl. Phys. Lett.* **2007**, *91*, 092109.

8. Abramowitz, M.; Stegun, I. A. *Handbook of Mathematical Functions* (Nat. Bureau of Standards Applied Mathematics Series 55, US Gov. Printing Office, Wash. DC, 1972), ch. 22.

INTENTIONALLY LEFT BLANK.

Appendix. Varactor Calculations

The derivatives of the function $f(z)$ are

$$f'(z) = -1 - \Lambda\left[\ln\left(1+e^{-z}\right) + \ln\left(1+e^{z}\right)\right]$$

$$f''(z) = -\Lambda\frac{e^{z}-1}{e^{z}+1}$$

$$f'''(z) = 2\Lambda\frac{e^{z}}{\left(e^{z}+1\right)^{2}}$$

$$f^{iv}(z) = 2\Lambda e^{z}\frac{e^{z}-1}{\left(e^{z}+1\right)^{3}}$$

$$f^{v}(z) = -2\Lambda e^{z}\frac{\left(e^{2z}-4e^{z}+1\right)}{\left(e^{z}+1\right)^{4}}$$

$$f^{vi}(z) = 2\Lambda e^{z}\frac{\left(e^{3z}-11e^{2z}+11e^{z}-1\right)}{\left(e^{z}+1\right)^{5}}$$

Let us expand the function $A(Z)$ in a power series in *Z* with unknown coefficients:

$$A(Z) = a_1 Z + a_2 Z^2 + a_3 Z^3 + a_4 Z^4 + a_5 Z^5 + a_6 Z^6 + \cdots$$

$$\Rightarrow \zeta_0 + Z = f\left(a_0\right) + Z\left[a_1 + a_2 Z + a_3 Z^2 + a_4 Z^3 + a_5 Z^4 + a_6 Z^5 + \cdots\right] f'\left(a_0\right)$$

$$+\frac{1}{2}Z^2\left[a_1 + a_2 Z + a_3 Z^2 + a_4 Z^3 + a_5 Z^4 + a_6 Z^5 + \cdots\right]^2 f''\left(a_0\right)$$

$$+\frac{1}{6}Z^3\left[a_1 + a_2 Z + a_3 Z^2 + a_4 Z^3 + a_5 Z^4 + a_6 Z^5 + \cdots\right]^3 f'''\left(a_0\right)$$

$$+\frac{1}{24}Z^4\left[a_1 + a_2 Z + a_3 Z^2 + a_4 Z^3 + a_5 Z^4 + a_6 Z^5 + \cdots\right]^4 f^{iv}\left(a_0\right)$$

$$+\frac{1}{120}Z^5\left[a_1 + a_2 Z + a_3 Z^2 + a_4 Z^3 + a_5 Z^4 + a_6 Z^5 + \cdots\right]^5 f^{v}\left(a_0\right)$$

$$+\frac{1}{720}Z^6\left[a_1 + a_2 Z + a_3 Z^2 + a_4 Z^3 + a_5 Z^4 + a_6 Z^5 + \cdots\right]^6 f^{vi}\left(a_0\right) + \cdots$$

We obtain the "operating point" of the varactor (*not* the dc component of *z*, due to self-bias effects) by numerically solving the implicit relation $\zeta_0 = f\left(a_0\right)$, which gives the first term a_0 in the dc charge density. We will look for frequency multiplication up to 6ω using this power series, i.e.,

$$\zeta = \zeta_0 + Z = \zeta_0 + \zeta_1 \cos\left(\omega t + \varphi\right) \Rightarrow z = \sum_{m=0}^{6} c_m \cos m\left(\omega t + \varphi\right)$$

where the c_m are unknown amplitudes. Then the charge density is

$$\sigma = \left(C_{gt} + C_{gb}\right)\frac{1}{\beta q}(\zeta + z) = \left(C_{gt} + C_{gb}\right)\frac{1}{\beta q}\left(\zeta_0 + c_0 + \left[\zeta_1 + c_1\right]\cos\left(\omega t + \varphi\right) + \sum_{m=2}^{6} c_m \cos m\left(\omega t + \varphi\right)\right)$$

Collecting powers of *Z* and matching coefficients on both sides of the expansions (with the help of *Mathematica*) lead to the following coefficient set $\left\{a_m\right\}$ for the series representation of $A(Z)$ out to 6th order in ζ_1:

$$\zeta_1 = a_1 f'\left(a_0\right) \Rightarrow a_1 = \frac{\zeta_1}{f'\left(a_0\right)}$$

$$0 = a_2 f'\left(a_0\right) + \frac{1}{2}{a_1}^2 f''\left(a_0\right) \Rightarrow a_2 = -\frac{1}{2}\left(\frac{1}{f'\left(a_0\right)}\right)^3 {\zeta_1}^2 f''\left(a_0\right)$$

$$0 = a_3 f'\left(a_0\right) + a_1 a_2 f''\left(a_0\right) + \frac{1}{6}{a_1}^3 f'''\left(a_0\right) \Rightarrow a_3 = \frac{1}{6}{\zeta_1}^3\left(\frac{1}{f'\left(a_0\right)}\right)^5\left[3 f''\left(a_0\right)^2 - f'\left(a_0\right) f'''\left(a_0\right)\right]$$

$$0 = a_4 f'\left(a_0\right) + \left\{\frac{1}{2}{a_2}^2 + a_1 a_3\right\} f''\left(a_0\right) + \frac{1}{6}{a_1}^2 a_2 f'''\left(a_0\right) + \frac{1}{24}{a_0}^5 f^{iv}\left(a_0\right)$$

$$\Rightarrow a_4 = -\frac{1}{24}{\zeta_1}^4\left(\frac{1}{f'\left(a_0\right)}\right)^7\left[15 f''\left(a_0\right)^3 - 10 f'\left(a_0\right) f''\left(a_0\right) f'''\left(a_0\right) + f'\left(a_0\right)^2 f^{iv}\left(a_0\right)\right]$$

$$0 = a_5 f'\left(a_0\right) + \left\{a_2 a_3 + a_1 a_4\right\} f''\left(a_0\right) + \frac{1}{2}\left\{a_1 {a_2}^2 + {a_1}^2 a_3\right\} f'''\left(a_0\right) + \frac{1}{6}{a_1}^3 a_2 f^{iv}\left(a_0\right) + \frac{1}{120}{a_1}^5 f^{v}\left(a_0\right)$$

$$\Rightarrow a_5 = \frac{1}{120}{\zeta_1}^5\left(\frac{\zeta_1}{f'\left(a_0\right)}\right)^9\left[\begin{array}{l} 105 f''\left(a_0\right)^4 - 105 f'\left(a_0\right) f''\left(a_0\right)^2 f'''\left(a_0\right) + 10 f'\left(a_0\right)^2 f'''\left(a_0\right)^2 \\ +15 f'\left(a_0\right)^2 f''\left(a_0\right) f^{iv}\left(a_0\right) - f'\left(a_0\right)^3 f^{v}\left(a_0\right) \end{array}\right]$$

$$0 = a_6 f'(a_0) + \left\{\frac{1}{2}{a_3}^2 + a_2 a_4 + a_1 a_5\right\} f''(a_0) + \left\{\frac{1}{6}{a_2}^3 + a_1 a_2 a_3 + \frac{1}{2}{a_1}^2 a_4\right\} f'''(a_0)$$
$$+ \left\{\frac{1}{2}{a_1}^2 a_4 + \frac{1}{4}{a_1}^2 {a_2}^2 + \frac{1}{6}{a_1}^3 a_3\right\} f^{iv}(a_0) + \frac{1}{24}{a_1}^4 a_2 f^{v}(a_0) + \frac{1}{720}{a_1}^6 f^{vi}(a_0)$$
$$\Rightarrow a_6 = -\frac{1}{720}\zeta_1{}^6 \left(\frac{\zeta_1}{f'(a_0)}\right)^{11} \left[\begin{array}{l} 945 f''(a_0)^5 - 1260 f'(a_0) f''(a_0)^3 f'''(a_0) \\ +280 f'(a_0)^2 f''(a_0) f'''(a_0)^2 + 210 f'(a_0)^2 f''(a_0)^2 f^{iv}(a_0) \\ -35 f'(a_0)^3 f'''(a_0) f^{iv}(a_0) - 21 f'(a_0)^3 f''(a_0) f^{v}(a_0) \\ + f'(a_0)^4 f^{vi}(a_0) \end{array}\right]$$

If the dimensionless voltage *Z* is a single frequency sinusoid, powers of *Z* are expressible as harmonics of the fundamental frequency via the relation

$$\cos n\omega t = T_n(\cos n\omega t)$$

where $T_n(x)$ are Chebyshev polynomials of the first kind, the first seven of which are *(8)*

$$T_0(x) = 1$$
$$T_1(x) = x$$
$$T_2(x) = 2x^2 - 1$$
$$T_3(x) = 4x^3 - 3x$$
$$T_4(x) = 8x^4 - 8x^2 + 1$$
$$T_5(x) = 16x^5 - 20x^3 + 5x$$
$$T_6(x) = 32x^6 - 48x^4 + 18x^2 - 1$$

Inverting these equations allows us to express simple powers as sums of Chebyshev polynomials:

$$
\begin{aligned}
1 &= T_0(x) \\
x &= T_1(x) \\
x^2 &= \frac{1}{2}T_0(x) + \frac{1}{2}T_2(x) \\
x^3 &= \frac{3}{4}T_1(x) + \frac{1}{4}T_3(x) \\
x^4 &= \frac{3}{8}T_0(x) + \frac{1}{2}T_2(x) + \frac{1}{8}T_4(x) \\
x^5 &= \frac{5}{8}T_1(x) + \frac{5}{16}T_3(x) + \frac{1}{16}T_5(x) \\
x^6 &= \frac{5}{16}T_0(x) + \frac{15}{32}T_2(x) + \frac{3}{16}T_4(x) + \frac{1}{32}T_6(x)
\end{aligned}
$$

Then

$$
a_0 + a_1x + a_2x^2 + a_3x^3 + a_4x^4 + a_5x^5 + a_6x^6 = \begin{pmatrix} a_0 & a_1 & a_2 & a_3 & a_4 & a_5 & a_6 \end{pmatrix} \begin{pmatrix} 1 \\ x \\ x^2 \\ x^3 \\ x^4 \\ x^5 \\ x^6 \end{pmatrix}
$$

$$
= \begin{pmatrix} a_0 & a_1 & a_2 & a_3 & a_4 & a_5 & a_6 \end{pmatrix} \begin{pmatrix} 1 & 0 & 0 & 0 & 0 & 0 & 0 \\ 0 & 1 & 0 & 0 & 0 & 0 & 0 \\ \frac{1}{2} & 0 & \frac{1}{2} & 0 & 0 & 0 & 0 \\ 0 & \frac{3}{4} & 0 & \frac{1}{4} & 0 & 0 & 0 \\ \frac{3}{8} & 0 & \frac{1}{2} & 0 & \frac{1}{8} & 0 & 0 \\ 0 & \frac{5}{8} & & \frac{5}{16} & 0 & \frac{1}{16} & 0 \\ \frac{5}{16} & 0 & \frac{15}{32} & 0 & \frac{3}{16} & 0 & \frac{1}{32} \end{pmatrix} \begin{pmatrix} T_0 \\ T_1 \\ T_2 \\ T_3 \\ T_4 \\ T_5 \\ T_6 \end{pmatrix}
$$

and so

$$\begin{pmatrix} a_0 & a_1 & a_2 & a_3 & a_4 & a_5 & a_6 \end{pmatrix} \begin{pmatrix} 1 & 0 & 0 & 0 & 0 & 0 & 0 \\ 0 & 1 & 0 & 0 & 0 & 0 & 0 \\ \frac{1}{2} & 0 & \frac{1}{2} & 0 & 0 & 0 & 0 \\ 0 & \frac{3}{4} & 0 & \frac{1}{4} & 0 & 0 & 0 \\ \frac{3}{8} & 0 & \frac{1}{2} & 0 & \frac{1}{8} & 0 & 0 \\ 0 & \frac{5}{8} & 0 & \frac{5}{16} & 0 & \frac{1}{16} & 0 \\ \frac{5}{16} & 0 & \frac{15}{32} & 0 & \frac{3}{16} & 0 & \frac{1}{32} \end{pmatrix}$$

$$= \begin{pmatrix} a_0 + \frac{1}{2}a_2 + \frac{3}{8}a_4 + \frac{5}{16}a_6 & a_1 + \frac{3}{4}a_3 + \frac{5}{8}a_5 & \frac{1}{2}a_2 + \frac{1}{2}a_4 + \frac{15}{32}a_6 & \frac{1}{4}a_3 + \frac{5}{16}a_5 & \frac{1}{8}a_4 + \frac{3}{16}a_6 & \frac{1}{16}a_5 & \frac{1}{32}a_6 \end{pmatrix}$$

defines the "conversion coefficients" for harmonic generation amplitudes:

$$c_0 = a_0 + \frac{1}{2}a_2 + \frac{3}{8}a_4 + \frac{5}{16}a_6$$
$$c_1 = a_1 + \frac{3}{4}a_3 + \frac{5}{8}a_5$$
$$c_2 = \frac{1}{2}a_2 + \frac{1}{2}a_4 + \frac{15}{32}a_6$$
$$c_3 = \frac{1}{4}a_3 + \frac{5}{16}a_5$$
$$c_4 = \frac{1}{8}a_4 + \frac{3}{16}a_6$$
$$c_5 = \frac{1}{16}a_5$$
$$c_6 = \frac{1}{32}a_6$$

For the dc component and linear susceptance we find explicitly that

$$\zeta_0 = f\left(a_0\right) \Rightarrow \zeta_0 + c_0 = f\left(a_0\right) + c_0 = -a_0 + \Lambda\left[F_1\left(-a_0\right) - F_1\left(a_0\right)\right] + a_0 + \frac{1}{2}a_2 + \frac{3}{8}a_4 + \frac{5}{16}a_6$$
$$= \Lambda\left[F_1\left(-a_0\right) - F_1\left(a_0\right)\right] + \frac{1}{2}a_2 + \frac{3}{8}a_4 + \frac{5}{16}a_6$$

$$\zeta_1 + c_1 = \zeta_1 + a_1 + \frac{3}{4}a_3 + \frac{5}{8}a_5 = \zeta_1\left(1 + \frac{1}{f'\left(a_0\right)}\right) + \frac{3}{4}a_3 + \frac{5}{8}a_5 = \frac{\Lambda\left[\ln\left(1+e^{-a_0}\right) + \ln\left(1+e^{a_0}\right)\right]}{1+\Lambda\left[\ln\left(1+e^{-a_0}\right) + \ln\left(1+e^{a_0}\right)\right]}\zeta_1 + \frac{3}{4}a_3 + \frac{5}{8}a_5$$

The frequency multiplication signals are $\sigma_m = \left(C_{gt} + C_{gb}\right)\frac{1}{\beta q}c_m$ with $m > 1$. Then

$$\Lambda = \frac{q^2}{C_{gt}+C_{gb}}\frac{2}{\pi\beta\left(\hbar\upsilon_F\right)^2} = \frac{\beta q}{C_{gt}+C_{gb}}\frac{2q}{\pi\left(\beta\hbar\upsilon_F\right)^2} \Rightarrow \frac{C_{gt}+C_{gb}}{\beta q} = \frac{2q}{\pi\Lambda\left(\beta\hbar\upsilon_F\right)^2}$$

$$\Rightarrow \sigma_m = \frac{2q}{\pi\Lambda}\left(\frac{kT}{\hbar\upsilon_F}\right)^2 c_m \equiv \sigma_0\frac{c_m}{\Lambda}$$

are the ac charge-density components.

NO. OF COPIES	ORGANIZATION
1 ELECT	ADMNSTR DEFNS TECHL INFO CTR ATTN DTIC OCP 8725 JOHN J KINGMAN RD STE 0944 FT BELVOIR VA 22060-6218
1 CD	OFC OF THE SECY OF DEFNS ATTN ODDRE (R&AT) THE PENTAGON WASHINGTON DC 20301-3080
1	US ARMY RSRCH DEV AND ENGRG CMND ARMAMENT RSRCH DEV & ENGRG CTR ARMAMENT ENGRG & TECHNLGY CTR ATTN AMSRD AAR AEF T J MATTS BLDG 305 ABERDEEN PROVING GROUND MD 21005-5001
1	PM TIMS, PROFILER (MMS-P) AN/TMQ-52 ATTN B GRIFFIES BUILDING 563 FT MONMOUTH NJ 07703
1	US ARMY INFO SYS ENGRG CMND ATTN AMSEL IE TD A RIVERA FT HUACHUCA AZ 85613-5300
1	COMMANDER US ARMY RDECOM ATTN AMSRD AMR W C MCCORKLE 5400 FOWLER RD REDSTONE ARSENAL AL 35898-5000
1	US GOVERNMENT PRINT OFF DEPOSITORY RECEIVING SECTION ATTN MAIL STOP IDAD J TATE 732 NORTH CAPITOL ST NW WASHINGTON DC 20402
1	US ARMY RSRCH LAB ATTN RDRL CIM G T LANDFRIED BLDG 4600 ABERDEEN PROVING GROUND MD 21005-5066

NO. OF COPIES	ORGANIZATION
4	US ARMY RSRCH LAB ATTN IMNE ALC HRR MAIL & RECORDS MGMT ATTN RDRL CIM L TECHL LIB ATTN RDRL CIM P TECHL PUB ATTN RDRL SER E F CROWNE ADELPHI MD 20783-1197

INTENTIONALLY LEFT BLANK.